FEATURE ARTICLE

Determination of the Local Structure and Electronic States of High-T_c Superconductors by Scanning Tunneling Microscopy

Zhe Zhang and Charles M. Lieber*

Department of Chemistry and Division of Applied Sciences, Harvard University, 12 Oxford Street, Cambridge, Massachusetts 02138 *(Received: August 21, 1991)*

To date, scanning tunneling microscopy (STM) has significantly advanced our understanding of the local structure, electronic properties, and reactivity of semiconductor surfaces. Less recognized is the fact that STM can also elucidate the local structural and electronic properties of low-dimensional materials. Herein, we demonstrate that STM can provide new and essential insight into the physical complexities of high-temperature copper oxide superconductors that is unavailable from conventional studies. After reviewing the basic theoretical concepts needed to evaluate STM data, we discuss several specific cases that illustrate the unique information that STM provides. These examples include (1) the atomic level nature of structural disorder in the BiO and TlO layers of $Bi_2Sr_2CaCu_2O_8$ and $Tl_2Ba_2CaCu_2O_8$ and the low-energy electronic states associated with these structural features, (2) the local structure and electronic consequences of metal substitution and oxygen doping in $Bi_2Sr_2CaCu_2O_8$, and (3) low-temperature tunneling spectroscopy measurements of the superconducting energy gap. Lastly, we summarize exciting future avenues to pursue in STM studies of these and other materials.

I. Introduction

Scanning tunneling microscopy (STM) is a uniquely powerful probe of local surface structure and electronic states which has advanced remarkably the understanding of metal and semiconductor interfaces.[1-6] Perhaps less recognized is the potential of STM as a technique for probing complex structural and electronic properties of bulk materials. To obtain data that is directly relevant to understanding bulk properties with a surface-sensitive technique requires, however, that the surface terminate with bulk structure and ideally "bulklike" bonding. While these constraints are not met at the surfaces of three-dimensional solids, low-dimensional materials, such as layered compounds, often cleave to yield unreconstructed van der Waals surfaces that are structurally and electronically similar to the bulk. Hence, it is expected that in these cases STM will provide key insight into structure and electronic states of the bulk. For example, STM investigations of low-dimensional metal chalcogenide materials have done much to advance the understanding of the charge density wave phases in these solids.[7,8] STM has been used to resolve longstanding questions about the structures of complicated incommensurate charge density wave phases[9] and to characterize directly for the first time the local interaction of impurities with a charge density wave.[10-12] In addition, a variation of STM, scanning tunneling spectroscopy (STS), has been used to characterize the magnitude of the charge density wave energy gap in several of these materials.[13]

The focus of this article is on recent and exciting applications of STM to the study of high-temperature copper oxide superconductors (HTSCs). These materials are highly anisotropic in that two-dimensional copper oxide planes are key structural elements in all of the different families of solids. Herein, studies of the $Bi_2Sr_2Ca_{n-1}Cu_nO_{2n+4}$ and $Tl_2Ba_2Ca_{n-1}Cu_nO_{2n+4}$ families will be specifically addressed. These materials consist of quasi-two-dimensional repeat units containing 2-BiO or TlO, 2-SrO or BaO, $(n-1)$Ca, and n-CuO_2 layers as illustrated for the $n = 2$ Bi-based material in Figure 1. The average structure is quite straightforward, although in reality these materials exhibit a wide range of structural complexities that are not yet well characterized. For example, the Bi/Tl families of materials show considerable disorder in the BiO and TlO layers, oxygen nonstoichiometry, and substitution of metals between the idealized layers shown in Figure 1.[14,15] The detailed nature of such local disorder is intrinsically difficult to address by conventional diffraction techniques as are the electronic consequences of these structural variations. A complete picture of the microscopic properties of these materials is, however, almost certainly necessary to understand high-temperature superconductivity when one considers that the structural disorder has a dimensionality similar to the superconducting pair coherence length.

To characterize in detail the structure and low-energy electronic states of the HTSCs we have been using STM, and below we summarize results from our laboratory on these systems. The paper is organized as follows: First, we will introduce key features of the tunneling microscope and the theoretical concepts needed to interpret the experimental data. The remainder of the article will focus on experimental studies, including (1) the structural and electronic nature of the BiO layer in single crystals of $Bi_2Sr_2CaCu_2O_8$, (2) the structural and electronic properties of the

* To whom correspondence should be addressed.

(1) Binnig, G.; Rohrer, H.; Gerber, C.; Weibel, E. *Phys. Rev. Lett.* **1982**, *49*, 57.
(2) Golovchenko, J. A. *Science* **1986**, *232*, 48.
(3) Tromp, R. M.; Hamers, R. J.; Demuth, J. E. *Science* **1986**, *234*, 304.
(4) Hamers, R. J. *Annu. Rev. Phys. Chem.* **1989**, *40*, 531.
(5) Griffith, J. E.; Kochanski, G. P. *Annu. Rev. Mater. Sci.* **1990**, *20*, 194.
(6) Avouris, P. *J. Phys. Chem.* **1990**, *94*, 2246.
(7) Coleman, R. V.; Giambattista, B.; Hansma, P. K.; Johnson, A.; McNairy, W. W.; Slough, C. G. *Adv. Phys.* **1988**, *37*, 559.
(8) Lieber, C. M.; Wu, X. L. *Acc. Chem. Res.* **1991**, *24*, 170.
(9) Wu, X. L.; Lieber, C. M. *Science* **1989**, *243*, 1703. Wu, X. L.; Lieber, C. M. *Phys. Rev. Lett.* **1990**, *64*, 1150.
(10) Wu, X. L.; Lieber, C. M. *J. Am. Chem. Soc.* **1989**, *111*, 2731. Chen, H.; Wu, X. L.; Lieber, C. M. *J. Am. Chem. Soc.* **1990**, *112*, 3326.
(11) Wu, X. L.; Zhou, P.; Lieber, C. M. *Phys. Rev. Lett.* **1988**, *61*, 2604. Wu, X. L.; Zhou, P.; Lieber, C. M. *Nature* **1988**, *335*, 55. Wu, X. L.; Lieber, C. M. *Phys. Rev. B* **1990**, *41*, 1239.
(12) Dai, H.; Chen, H.; Lieber, C. M. *Phys. Rev. Lett.* **1991**, *66*, 3183.
(13) Wang, C.; Giambattista, B.; Slough, C. G.; Coleman, R. V. *Phys. Rev. B* **1990**, *42*, 8890.
(14) Rao, C. N. R.; Raveau, B. *Acc. Chem. Res.* **1989**, *22*, 106.
(15) Torardi, C. C.; Subramanian, M. A.; Calabrese, J. C.; Gopalakrishnan, J.; Morrissey, K. J.; Askew, T. R.; Flippen, R. B.; Chowdhry, U.; Sleight, A. W. *Science* **1988**, *240*, 631.

0022-3654/92/2096-2030$03.00/0

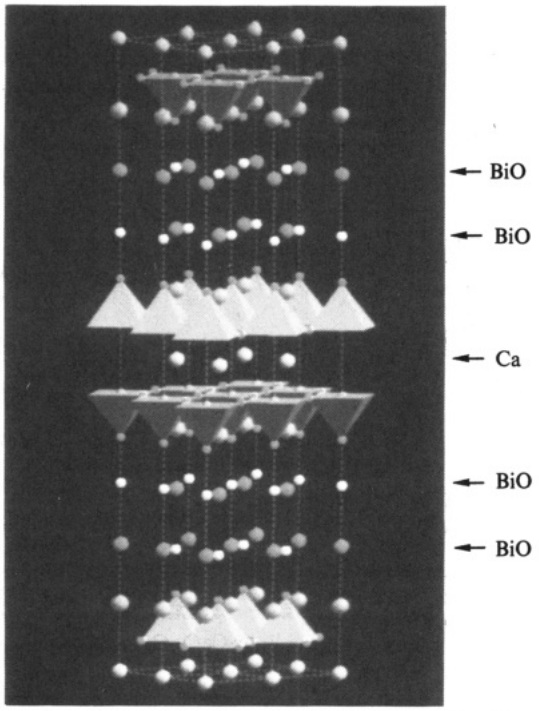

Figure 1. Structural view of $Bi_2Sr_2CaCu_2O_8$ highlighting the quasi-two-dimensional nature of this solid. Crystals cleave preferentially between the Bi–O double layers in the structure (*a*–*b* plane); the CuO planes correspond to the bases of the square pyramid polyhedra and are separated by Ca^{2+} ions. The *c* axis is vertical with respect to the page in this model.

TlO layer in $Tl_2Ba_2Ca_{n-1}Cu_nO_{2n+4}$ crystals, (3) the microscopic and macroscopic role of Pb substitution in $Pb_xBi_{2-x}Sr_2CaCu_2O_8$ materials, (4) the effects of oxygen doping in $Bi_2Sr_2CaCu_nO_{8+\delta}$ crystals, and (5) low-temperature tunneling spectroscopy measurements of the superconducting energy gap.

II. STM: Experiment and Theory

In this section we briefly review the instrumentation and theoretical concepts that are essential for understanding the STM studies which will be discussed later. More detailed reviews can be found elsewhere.[4,16–18] A typical microscope is illustrated schematically in Figure 2. The underlying basis for the operation of the microscope is electron tunneling between a sharp metal tip and a conducting sample. When the tip and sample are brought sufficiently close, their wave functions can overlap. If a bias voltage V is then applied to the sample, a tunneling current I will flow between the sample and tip. Electrons will tunnel from filled electronic states in the tip to empty states in the sample when V is positive, and conversely, electrons will tunnel from filled sample states to empty tip states when V is negative (Figure 2, inset). The tunneling current that flows when V is applied varies exponentially with the tip–sample separation, and for a typical work function of 4 eV I decreases 10-fold for an angstrom increase in separation. The actual decay rate can, however, vary significantly with the barrier properties. The strong exponential dependence of the tunneling current on distance enables STM to achieve high vertical resolution. An atomic resolution map of the surface can then be generated by rastering the tip over the sample with angstrom-level control using piezoceramic positioners. Experimental images are typically acquired in the constant current mode in which a feedback loop controls the vertical position of the tip above the sample so that I is equal to a reference current (I_{ref}) at all coordinates on the surface. Features in constant current mode images thus correspond to vertical displacements of the piezo positioner needed to maintain a constant tunneling current.

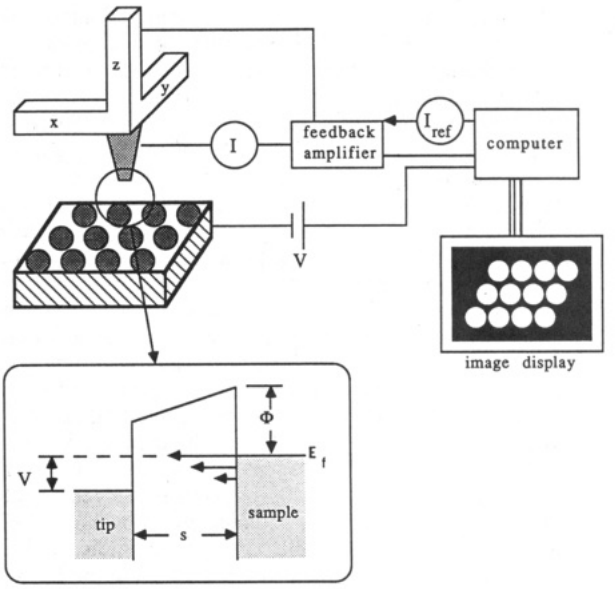

Figure 2. Schematic illustration of a tunneling microscope. The inset is a one-dimensional representation of tunneling between a metallic sample and tip where *s* is the tip–sample separation and *V* is the applied voltage.

Essential to the interpretation of such STM data is an understanding of the response of the tunneling current to the barrier properties, applied voltage, etc.; insight into these problems can be obtained from theoretical analyses of the tunneling problem.[19–23] As first discussed by Tersoff and Hamann, an expression for I can be readily derived by assuming unperturbed sample and tip wave functions and then using perturbation theory.[19] In the limit of small bias voltage and low temperature this treatment yields

$$I = (2\pi/\hbar)e^2V\sum|M_{st}|^2\delta(E_s-E_f)\delta(E_t-E_f) \quad (1)$$

where M_{st} is the tunneling matrix element between wave functions on the tip ψ_t and sample ψ_s. As shown by Bardeen,[24] the tunneling matrix can be written

$$M_{st} = (\hbar^2/2m)\int(\psi_t^*\nabla\psi_s - \psi_s\nabla\psi_t^*)\,dS \quad (2)$$

where the integral corresponds to a surface within the barrier region between the sample and tip. To evaluate M_{st} in a way that the resulting expression for I can be compared quantitatively to STM images in general (i.e., not for one specific choice of sample and tip) requires several approximations. Tersoff and Hamann showed that, by assuming the tip was as a locally spherical potential well with only s wave functions, I could be expressed as

$$I \propto \sum_s|\psi_s(r_0)|^2\delta(E_s-E_f) \quad (3)$$

By definition, the summation is the local density of sample electronic states, $\rho(r_0,E)$, at the center of curvature of the tip

$$\rho(r_0,E) \equiv \sum_s|\psi_s(r_0)|^2\delta(E_s-E_f) \quad (4)$$

and thus constant current images correspond to *contours of constant density of sample electronic states*.

In view of the simplicity of this result it is useful to consider the effect of the approximations made in deriving eq 4. Treatment

(16) Hansma, P. K.; Tersoff, J. *J. Appl. Phys.* **1987**, *61*, R1. Hansma, P. K.; Elings, V. B.; Marti, O.; Bracker, C. E. *Science* **1988**, *242*, 209.
(17) Kuk, Y.; Silverman, P. J. *Rev. Sci. Instrum.* **1989**, *60*, 165.
(18) Sakurai, T.; Hashizume, T.; Kamiya, I.; Hasegawa, Y.; Sano, N.; Pickering, H. W.; Sakai, A. *Prog. Surf. Sci.* **1990**, *33*, 3.
(19) Tersoff, J.; Hamann, D. R. *Phys. Rev. Lett.* **1983**, *50*, 1998. Tersoff, J.; Hamann, D. R. *Phys. Rev. B* **1985**, *31*, 805.
(20) Lang, N. D. *Phys. Rev. Lett.* **1986**, *56*, 1164; *Phys. Rev. B* **1986**, *34*, 5947.
(21) Selloni, A.; Carnevalli, P.; Tosatti, P. E.; Chen, C. D. *Phys. Rev. B* **1986**, *33*, 5770.
(22) Tersoff, J. *Phys. Rev. B* **1990**, *41*, 1235.
(23) Chen, C. J. *Phys. Rev. Lett.* **1990**, *65*, 448.
(24) Bardeen, J. *Phys. Rev. Lett.* **1963**, *6*, 57.

of the tip as a spherical potential is reasonable from the standpoint that in almost all cases the experimental tip shape is unknown, although it probably terminates in a cluster of atoms; i.e., the tip is approximately spherical. The s wave function approximation for the tip is more significant since it leads to a cancellation in (2) such that I depends only on the square of the sample wave function. Recently, Tersoff has examined more general descriptions of the tip and has found that for metals constant current images still correspond to contours of constant density of *sample* electronic states.[22] STM images of semiconductor surfaces at low V could, however, deviate significantly from this simple picture since only a small pocket of the surface Brillouin zone contributes to the tunneling. This deviation is limited, however, to the lowest Fourier component of the image, and thus the s wave function tip model may still be used in many cases to interpret images. In contrast, Chen has suggested that the s wave function approximation is unable to explain the resolution obtained in many experiments and has suggested that the tip function should be taken as a p_z or d_{z^2} dangling-bond state.[23] Using this tip model, he has been able to consistently explain atomic resolution images of close-packed metal surfaces. While these results indicate that significant progress has been made in understanding the role of tip, it will be important in the future to develop further these theoretical models so that experimental data can be quantitatively interpreted.

In the previous section we showed for reasonable approximations that constant current STM images correspond to contours of constant local density of sample electronic states. We now examine the tunneling current expression further to determine the explicit dependence of I on tip–sample separation and V. First, accounting for the exponential decay of the sample and tip wave functions into the tunneling gap, we can rewrite (3) as

$$I \propto \sum_s |\psi_s|^2 \exp(-2\kappa(R + s))\delta(E_s - E_f) \tag{5}$$

where R is the radius of the tip and s is the tip–sample separation. The decay parameter κ can be written as

$$\kappa = [(2m\phi/\hbar^2) + k^2]^{1/2} \tag{6}$$

where ϕ is the average work function and k is the parallel wavevector component of ψ_s. For the case of tunneling between planar, free-electron metal electrodes at small bias (i.e., $V \ll \phi$), eq 5 can be written as

$$I \propto (V/s) \exp(-2\kappa s) \tag{7}$$

with $\kappa = 1.025\sqrt{\phi}$.[25] Considering only the dominant exponential part of eq 7, we can express the work function as

$$\phi = 0.952(\mathrm{d} \ln I/\mathrm{d}s)^2 \tag{8}$$

Equation 8 indicates that the work function can be determined by measuring the distance dependence of the tunneling current; however, it should be recognized that the derivation of (8) does not consider modifications of the barrier due to the close proximity of the two electrodes (i.e., the STM tip and sample). Significantly, Lang has recently shown that the slow decay of the exchange correlation potential causes the apparent work function to be less than the true sample work function for electrode separations appropriate to the STM experiment.[26] Hence, the barrier height measured by STM is generally smaller than the sample work function.

In addition, we consider tunneling simultaneously from two distinct layers in a solid such as the BiO and CuO layers of $Bi_2Sr_2CaCu_2O_8$ (Figure 1). If we assume that the work functions of layer 1 and layer 2 are the same, then the ratio of the tunneling currents (I_1/I_2) from these layers is

$$I_1/I_2 = \exp(-1.025\sqrt{\phi}(s_2 - s_1)) \tag{9}$$

This result shows that if the density of states (DOS) of the two layers are similar, but layer 2 is 3 Å below a surface comprised of layer 1, then the tunneling contribution from layer 2 can be neglected. However, when the DOS differ significantly for the two layers this simplification may be inappropriate.

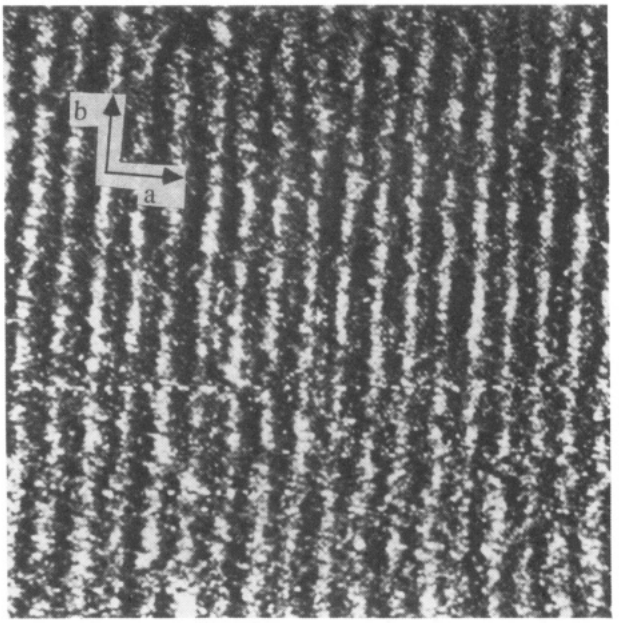

Figure 3. A 480 × 480 Å^2 image of $Bi_2Sr_2CaCu_2O_8$ recorded with a bias voltage of 250 mV and a tunneling current of 0.6 nA.

Lastly, we analyze the response of I to variations in V at fixed tip–sample separation. Since I is proportional to the local density of sample electronic states (LDOS), it was proposed early on that I–V data could provide a direct measure of the LDOS versus energy. Since the wave function decay depends on V, eq 3 should be rewritten as

$$I \propto \int \rho(r,E)\ T(E,\mathrm{eV})\ \mathrm{d}E \tag{10}$$

where $T(E,\mathrm{eV})$ is the transmission probability that takes into account the energy (eV)-dependent wave function decay. In this expression it is assumed that the density of tip states do not vary significantly with energy. In the limit of small bias, $\mathrm{d}I/\mathrm{d}V \propto$ LDOS (i.e., the typical assumption for conventional tunneling spectroscopy); however, for finite bias the exponential dependence of $T(E,\mathrm{eV})$ on V becomes important. As shown by Feenstra and co-workers,[27] this exponential dependence can be effectively removed by normalizing $\mathrm{d}I/\mathrm{d}V$ by V/I, that is

$$(V/I)\ \mathrm{d}I/\mathrm{d}V \propto \mathrm{LDOS} \tag{11}$$

Comparisons of the LDOS data obtained by STS with photoemission and inverse photoemission results show that the approximations made in arriving at (11) are reasonable. It should be noted that STS data typically only provide a qualitative measure of the LDOS, although it is hoped that further theoretical work will overcome this shortcoming in the future. With this background in hand we now turn to our STM studies of the HTSC materials.

III. The BiO Layer of $Bi_2Sr_2CaCu_2O_8$

The family of HTSC materials $Bi_2Sr_2Ca_{n-1}Cu_nO_{2n+4}$ exhibits a variety of fascinating chemical and physical phenomena.[28-34]

(25) Simmons, J. *J. Appl. Phys.* **1963**, *34*, 1793.
(26) Lang, N. D. *Phys. Rev. B* **1988**, *37*, 10395.

(27) Feenstra, R. M.; Stroscio, J. A.; Fein, A. P. *Surf. Sci.* **1987**, *181*, 295.
(28) Whangbo, M.-H.; Torardi, C. C. *Acc. Chem. Res.* **1991**, *24*, 127.
(29) Sleight, A. W. *Science* **1988**, *242*, 1539.
(30) Ramakrishnan, T. V.; Rao, C. N. R. *J. Phys. Chem.* **1989**, *93*, 4414.
(31) Subramanian, M. A.; Torardi, C. C.; Calabrese, J. C.; Gopalakrishnan, J.; Morrissey, K. J.; Askew, T. R.; Flippen, R. B.; Chowdhry, U.; Sleight, A. W. *Science* **1988**, *239*, 1015. Gao, Y.; Lee, P.; Coppens, P.; Subramanian, M. A.; Sleight, A. W. *Science* **1988**, *241*, 954.
(32) Zandbergen, H. W.; Groen, W. A.; Mijlhoff, F. C.; van Tendeloo, G.; Amelinckx, S. *Physica C (Amsterdam)* **1988**, *156*, 325.

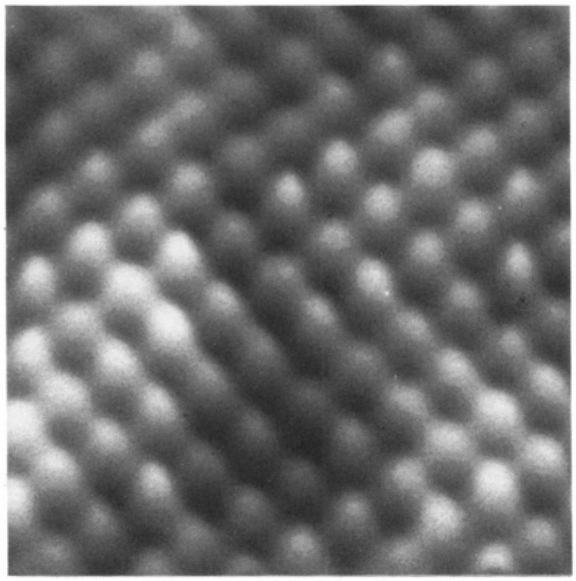

Figure 4. A 40 × 40 Å^2 atomic resolution image of $Bi_2Sr_2CaCu_2O_8$ recorded with a bias voltage of 200 mV and a tunneling current of 1.0 nA.

Structurally, these materials are the most anisotropic of the copper oxide superconductors due to several key features, including (1) the two-dimensional character of the BiO and CuO sheets within each repeat unit (Figure 1) and (2) the extremely weak coupling between the widely spaced (i.e., >3 Å) BiO layers in adjacent repeat units.[31] Notably, the weak bonding between adjacent BiO layers provides a natural cleavage plane in crystals of these materials.[35,36] Since covalent bonds are not broken when cleaving BiO/BiO double layers, the exposed BiO surface layer does not reconstruct, and hence the STM experiment probes the structure and electronic properties of a BiO layer similar to that found in the bulk.

A large area gray scale image of the BiO layer of a cleaved $Bi_2Sr_2CaCu_2O_8$ (T_c = 85 K) crystal is shown in Figure 3. This image exhibits a one-dimensional superstructure with an average modulation of 26 Å along the *a* axis. Images acquired simultaneously with positive (empty sample electronic states) and negative bias voltages (filled sample states) show the same features. These bias voltage dependent images demonstrate that the observed superstructure approximates the variation in the total density of states, and hence we can conclude that it is a structural feature. Bulk X-ray and electron diffraction studies[31-34] show a similar modulation and thus support our conclusion. A number of models have been proposed to explain the origin of this unique structural modulation in $Bi_2Sr_2CaCu_2O_8$; these are (1) lattice mismatch between the BiO and CuO layers, (2) extra oxygen substituted into the BiO layer which causes it to periodically buckle, and (3) periodic Cu or Sr substitution for Bi in the BiO layer.[31-34] At least three problems intrinsic to these materials have hampered diffraction-based efforts to elucidate the origin of this structure. First, the superstructure period is incommensurate with respect to the lattice. Second, the BiO layer has considerable disorder, and third, the X-ray and electron scattering cross sections for oxygen are significantly smaller than Bi. STM is not limited by these problems and can therefore provide unique insight into the origin and effects of this modulation.[35-39]

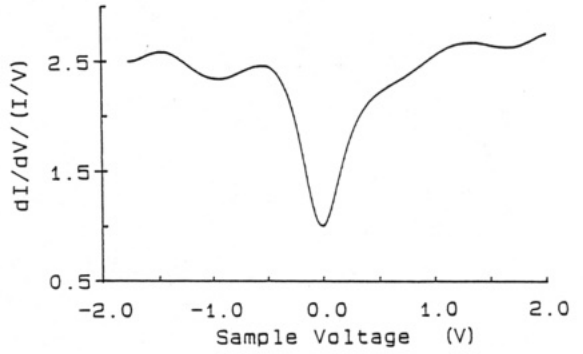

Figure 5. Plot of the normalized conductivity vs sample bias for a $Bi_2Sr_2CaCu_2O_8$ sample. The voltage corresponds to the energy relative to E_f (V = 0).

For example, analysis of real space STM images such as Figure 3 shows that the superstructure period is not a sinusoidal modulation. The period varies from 22 to 27 Å, and the distribution of periods about the average is broad and non-Gaussian.[36] These results strongly indicate that the superstructure is not due simply to BiO/CuO lattice mismatch (which would yield a sinusoidal modulation) but must have some substitutional component that causes local fluctuations in the superstructure period. Further evidence for the importance of substitution in determining the properties of the superstructure will be discussed below in the context of our studies of metal and oxygen doping in this system.

Large area images clearly indicate that substitution must play a role in the one-dimensional superstructure. In principle, atomically resolved images of the BiO lattice sites should resolve in detail the substitutional contribution to the modulation. A typical high-resolution image is shown in Figure 4. The atomic structure in this image has tetragonal symmetry with a period of 3.8 Å. This distance is consistent with both the average Bi–Bi and O–O distances determined by crystallography, and hence this data cannot be used to unambiguously define the complete atomic structure associated with the superstructure modulation. The atomic resolution images do show, however, that there can be significant positional disorder in the BiO layer which we suggest reflects inhomogeneous substitution in the BiO layer. We are currently investigating this proposal by probing the dependence of the local BiO structure on crystal composition and growth conditions.

The observation of alternate atomic sites indicates that the BiO layer is not metallic; i.e., the DOS are not delocalized over both lattice sites. To characterize directly the electronic character of the BiO layer, we and others have carried out tunneling spectroscopic measurements.[36-39] In contrast to other electronic spectroscopies such as photoemission, STM should provide a good measure of the BiO layer electronic states and not a convolution of both BiO and CuO layers. Such data is essential to develop models of the electronic structure for this system. Normalized conductivity versus voltage curves obtained with a feedback stabilized tunneling resistance of 10^9 Ω are shown in Figure 5. An important feature exhibited by these spectroscopic data is the apparent gap in the DOS at the Fermi level (E_f). Such data is reproducible on as grown T_c = 85 K crystals and indicates that the BiO layer is semiconducting in these materials. In contrast, band structure calculations using the full-potential linearized augmented plane wave method have suggested that the BiO layer is metallic,[40] although these calculations do not consider the superstructure and other structural disorder present in the BiO layer. Interestingly, recent tight-binding calculations indicate that

(33) Bordet, P.; Capponi, J. J.; Chaillout, C.; Chenavas, J.; Hewat, A. W.; Hewat, E. A.; Hodeau, J. L.; Marezio, M. *Stud. High Temp. Supercond.* **1989**, *2*, 171.
(34) Eibl, O. *Physica C (Amsterdam)* **1991**, *175*, 419.
(35) Kirk, M. D.; Nogami, J.; Baski, A. A.; Mitzi, D. B.; Kapitulnik, A.; Geballe, T. H.; Quate, C. F. *Science* **1988**, *242*, 1673.
(36) Wu, X. L.; Zhang, Z.; Wang, Y. L.; Lieber, C. M. *Science* **1990**, *248*, 1211.
(37) Tanaka, M.; Takahashi, T.; Katayama-Yoshida, H.; Yamazaki, S.; Fujinami, M.; Okabe, Y.; Mizutani, W.; Ono, M.; Kajimura, K. *Nature* **1989**, *339*, 691.
(38) Zhang, Z.; Wang, Y. L.; Wu, X. L.; Huang, J. L.; Lieber, C. M. *Phys. Rev. B* **1990**, *42*, 1082. Zhang, Z.; Zhao, N.; Lieber, C. M. *Proc. First Grad. Symp., Buffalo* **1991**, 57.
(39) Shih, C. K.; Feenstra, R. M.; Chandrashekhar, G. V. *Phys. Rev. B* **1991**, *43*, 7913. Shih, C. K.; Feenstra, R. M.; Kirtly, J. R.; Chandrashekhar, G. V. *Phys. Rev. B* **1989**, *40*, 2682.
(40) Massidda, S.; Yu, J.; Freeman, A. J.; Krakauer, H.; Pickett, W. E. *Phys. Rev. Lett.* **1988**, *60*, 1665.

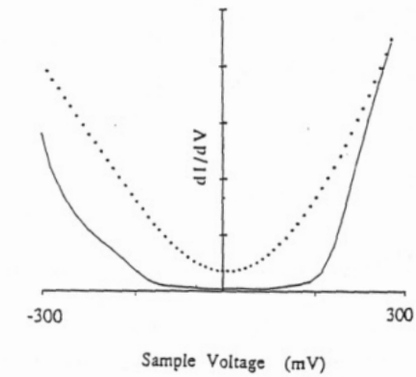

Figure 6. Conductance vs voltage curves recorded at two different tip–sample separations. The solid line was recorded with a tunneling resistance of 10^9 Ω, while the dashed line was measured with a tunneling resistance of 10^8 Ω.

distortions in the BiO layer raise the energy of the Bi-derived band above E_f and thus drive this layer to a semiconducting state.[41]

To probe further the electronic nature of the BiO layer, we have investigated the distance dependence of the LDOS. In preliminary work we found that STS measurements made at tip–sample separations closer than used to record Figure 5 showed a finite DOS at E_f.[38] More systematic measurements made in our group[38] and elsewhere[39] confirm this report (Figure 6). Specifically, when the tip is moved ≈2 Å closer to the sample, our data show that the conductivity only equals zero at the origin. These results demonstrate for small tip–sample separations that there is no apparent gap in the DOS; i.e., the BiO layer appears weakly metallic. One explanation that we have suggested for these observations is that the metallic states correspond to a tunneling contribution from the CuO layer that is 4.5 Å below the surface.[38] Alternatively, it is possible that the surface wave function has an unusually short decay length (i.e., due to $k > 0$). The apparent work function obtained from our experimental I–s data is 2.7 eV. This decay length is not unusually short, and thus we believe that this alternative hypothesis is unlikely. To obtain a tunneling contribution from the CuO layer, we estimate using (9) that there must be $\approx 10^3$ greater state density on this layer than on the BiO layer. While adequate calculations are not yet available to confirm this estimate, it is consistent with the known metallic character of the CuO layer. These results are significant in at least two other respects. First, they show that STM, in contrast to our usual expectations, can be sensitive to atomic layers lying below the surface. Second, these data indicate that it should be possible using STM to probe the electronic properties of the CuO layer "buried" beneath the BiO surface.

IV. The TlO Layer of $Tl_2Ba_2CaCu_2O_8$

We now turn from $Bi_2Sr_2CaCu_2O_8$ to the nearly isostructural family of HTSCs $Tl_2Ba_2Ca_{n-1}Cu_nO_{2n+4}$. These materials are derived from the Bi family simply by replacing Bi with Tl and Sr with Ba. In general, the average atomic structures of the Tl-based materials are similar to the Bi systems, although there are several important differences, including (1) the Tl materials do not exhibit a regular one-dimensional superstructure and (2) the bonding between adjacent TlO layers is significantly stronger.[28,42] Despite the stronger bonding between the TlO double layers, we have found that crystals of $Tl_2Ba_2CaCu_2O_8$ and $Tl_2Ba_2Ca_2Cu_3O_{10}$ cleave predominantly between the TlO double layers to expose a TlO surface in a manner analogous to $Bi_2Sr_2CaCu_2O_8$.[43,44] There are, however, significant differences in the atomic structure and electronic properties of the TlO versus BiO layers.

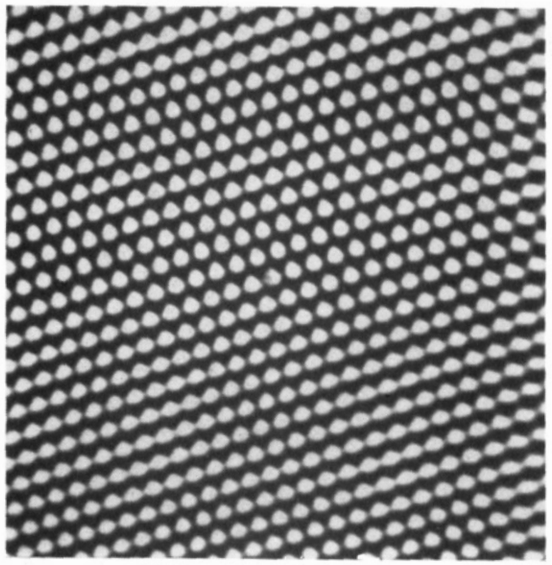

Figure 7. A 60 × 60 Å^2 image of a $Ti_2Ba_2CaCu_2O_8$ single crystal recorded with a bias voltage of −165 mV and a tunneling current of 1.9 nA. The near-trigonal lattice has a period of 2.4 Å.

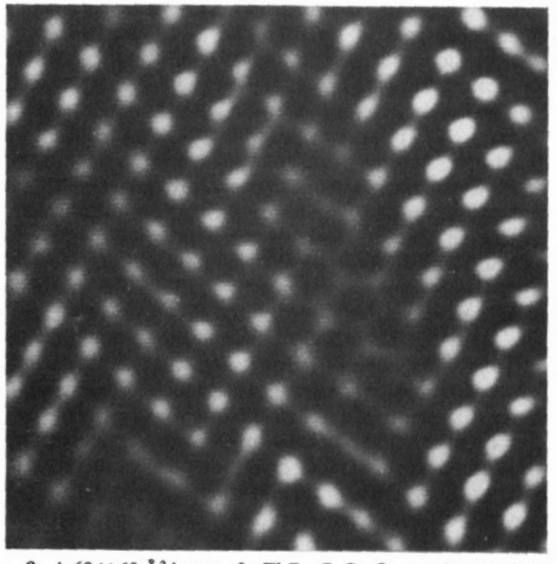

Figure 8. A 60 × 60 Å^2 image of a $Tl_2Ba_2CaCu_2O_8$ sample recorded with a bias voltage of −320 mV and a tunneling current of 2.1 nA. The structure observed in this image has a period of ≈4 Å.

An atomic resolution image of a cleaved $Tl_2Ba_2CaCu_2O_8$ crystal is shown in Figure 7. Similar images are observed over ≈90% of the surfaces of crystals that have broad superconducting transitions. The surface atomic structure has near trigonal symmetry with $a \approx b = 2.4 \pm 0.2$ Å and an a–b lattice angle of 65 ± 5°. The 2.4-Å average peak separation observed in our images is similar to the average in-plane TlO distance reported in X-ray diffraction studies[42] and differs significantly from the 1.93-Å CuO and 2.77-Å BaO in-plane separations. Hence, we have assigned the features in the images to the Tl and O lattice sites.[43,44] The surface TlO structure shown in Figure 7 is, however, highly distorted from the average tetragonal crystal symmetry. This distortion could reflect intrinsic disorder in the TlO layer that has been detected by X-ray and neutron diffraction and/or a surface reconstruction. Although additional studies are needed to clarify this symmetry issue, the observation of both atomic sites in these images demonstrates that Tl and O sites make a comparable contribution to the density of states near the Fermi level. Hence, it is apparent that the distorted structure does not adversely affect

(41) Torardi, C. C.; Jung, D.; Kang, D. B.; Ren, J.; Whangbo, M.-H. *Mater. Res. Soc. Symp. Proc.* **1989**, *156*, 295.
(42) Cox, D. E.; Torardi, C. C.; Subramanian, M. A.; Gopalakrishnan, J.; Sleight, A. W. *Phys. Rev. B* **1988**, *38*, 6624.
(43) Wu, X. L.; Lieber, C. M.; Ginley, D. S.; Gaughman, R. J. *Appl. Phys. Lett.* **1989**, *55*, 2129.
(44) Zhang, Z.; Lieber, C. M.; Ginley, D. S.; Baughman, R. J.; Morosin, B. *J. Vac. Sci. Technol. B* **1991**, *9*, 1009.

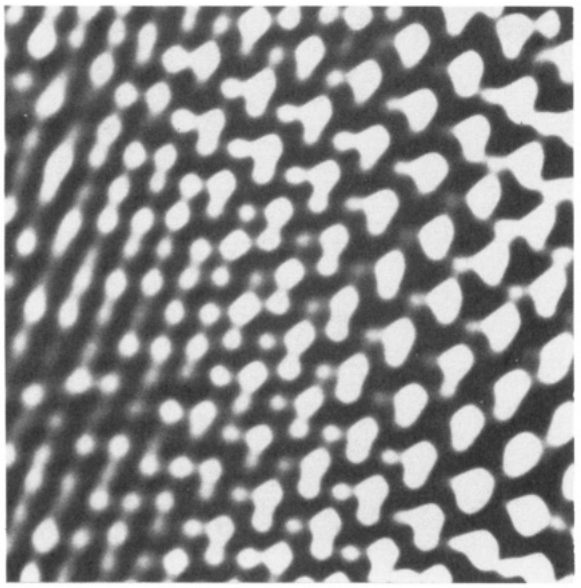

Figure 9. A 40 × 40 Å^2 image of $Tl_2Ba_2CaCu_2O_8$ that exhibits both types of structure; the lattice period on the left is 2.4 Å and on the right is 4 Å.

the formation of covalent TlO bonds and a metallic band. Interestingly, electronic structure calculations indicate that Tl and O will contribute unequally to the DOS near E_f for an undistorted structure but will form a delocalized metallic band when this layer distorts.[45]

Images of these same $Tl_2Ba_2CaCu_2O_8$ crystals also exhibit tetragonal structure with a period of ≈4 Å over about 10% of the surface (Figure 8). The localized and random occurrence of this tetragonal structure indicates that it is due to compositional inhomogeneities in the TlO layer. Further insight into the nature of this structure can be obtained from the analysis of images exhibiting both 4- and 2.4-Å structure (Figure 9). These data show that the two structural regions are not separated by an abrupt boundary or defect, but rather, there is a gradual decrease in the tunneling contribution from atomic sites across the 2.4- and 4-Å boundary. These results indicate that the electronic structure becomes more localized in the 4-Å region, and thus we have suggested that this structure may be assigned to either Tl–Tl or O–O sites as in images of the BiO layer. In addition, recent measurements in our laboratory have shown that this undistorted tetragonal structure is observed exclusively in images recorded on high-quality crystals (i.e., those exhibiting sharp superconducting transitions). The distorted 2.4-Å structure is observed, however, on samples that show broad superconducting transitions characteristic of compositional inhomogeneities.[46]

Spatially resolved spectroscopy measurements have also been made to characterize better the electronic properties of these two structurally distinct regions (Figure 10). The $(V/I)\,dI/dV$ data obtained on areas exhibiting the 2.4-Å structure *do not* exhibit a gap in DOS at E_f, although the DOS is lower than expected for a good metal. In contrast, there is a distinct gap in the DOS determined over regions with the 4-Å tetragonal atomic structure. These data confirm our interpretation of the TlO electronic structure inferred from the images and, furthermore, highlight the structural and electronic similarity of the tetragonal TlO regions with the 4-Å lattice constant to the BiO structure in $Bi_2Sr_2CaCu_2O_8$. As indicated above, these data are consistent with theoretical calculations which indicate that distortions in the TlO layer are essential for making this layer metallic. Significantly, we note that the metallic TlO structure can be associated with compositionally inhomogeneous samples which exhibit poor superconducting properties. Hence, we believe that distortions

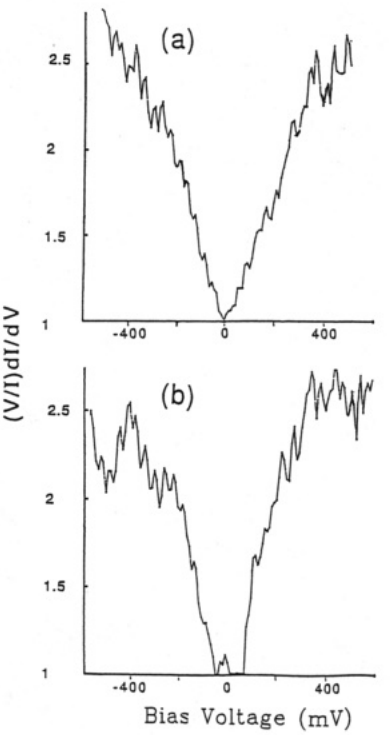

Figure 10. $(V/I)\,dI/dV$ vs V data obtained on (a) the 2.4-Å structural region and (b) the 4-Å structural region. The normalized conductivity curves, $(V/I)\,dI/dV$, were obtained by numerically differentiating I–V data.

in the TlO layer are deleterious to superconductivity in this system.

V. Pb Substitution in $Bi_2Sr_2CaCu_2O_8$

Metal substitution in HTSCs has been used extensively to probe factors that determine superconductivity and to prepare new materials. A well-studied example is Pb substitution for Bi in the BiO layers of the Bi-based materials. Since it was first reported that Pb substitution enhances the onset of superconductivity from 85 to 107 K in multiphase ceramic materials,[47] numerous investigations of this chemical modification have been reported. In ceramic $(BiPb)_2Sr_2Ca_{n-1}Cu_nO_{2n+4}$ materials Pb substitution has been found to favor formation of the $n = 3$ ($T_c = 110$ K) phase versus the $n = 2$ ($T_c = 85$ K) phase, although the average lattice parameters and transition temperatures for a given phase do not vary substantially. A detailed microscopic picture of the structural and electronic effects of Pb substitution has not, however, been put forth.

As part of a general program to develop a detailed microscopic understanding of the effects of doping in HTSCs, which is necessary to design rationally new systems, we have been using STM to characterize the atomic scale structural and electronic changes affected by substitution. In the case of Pb substitution, STM is an especially ideal probe since Pb primarily replaces Bi in the BiO layers and the $Pb_xBi_{2-x}Sr_2CaCu_2O_8$ crystals can be cleaved to expose a Bi(Pb)O layer directly at the surface. The unique capability of STM to probe both structural and electronic variations on the angstrom scale is particularly important in these short coherence length superconductors since metal substitution may cause short-range electronic disorder that will affect pairing.

Representative STM images of $x(Pb) = 0.3$ and $x(Pb) = 0.7$ single crystals are shown in Figure 11. In general, images of the $x(Pb) = 0.3$ samples exhibit a one-dimensional superstructure similar to that observed for $Bi_2Sr_2CaCu_2O_8$, whereas images of the $x(Pb) = 0.7$ samples do not show a periodic structural modulation. Analysis of the STM images of $x(Pb) = 0.3$ materials

(45) Yu, J.; Massidda, S.; Freeman, A. J. *Physica C* **1988**, *152*, 152. Jung, D.; Whangbo, M.-H.; Herron, N.; Torardi, C. C. *Physica C* **1989**, *160*, 381.

(46) Zhang, Z.; Chen, C. C.; Lieber, C. M.; Morosin, B.; Venturini, E. L.; Ginley, D. S. *Phys. Rev. B*, in press.

(47) Sunshine, S. A.; Siegrist, T.; Schneemeyer, L. F.; Murphy, D. W.; Cava, R. J.; Batlogg, B.; van Dover, R. B.; Fleming, R. M.; Glarum, S. H.; Nakahara, S.; Farrow, R.; Krajewski, J. J.; Zahurak, S. M.; Waszczak, J. V. *Phys. Rev. B* **1988**, *38*, 893.

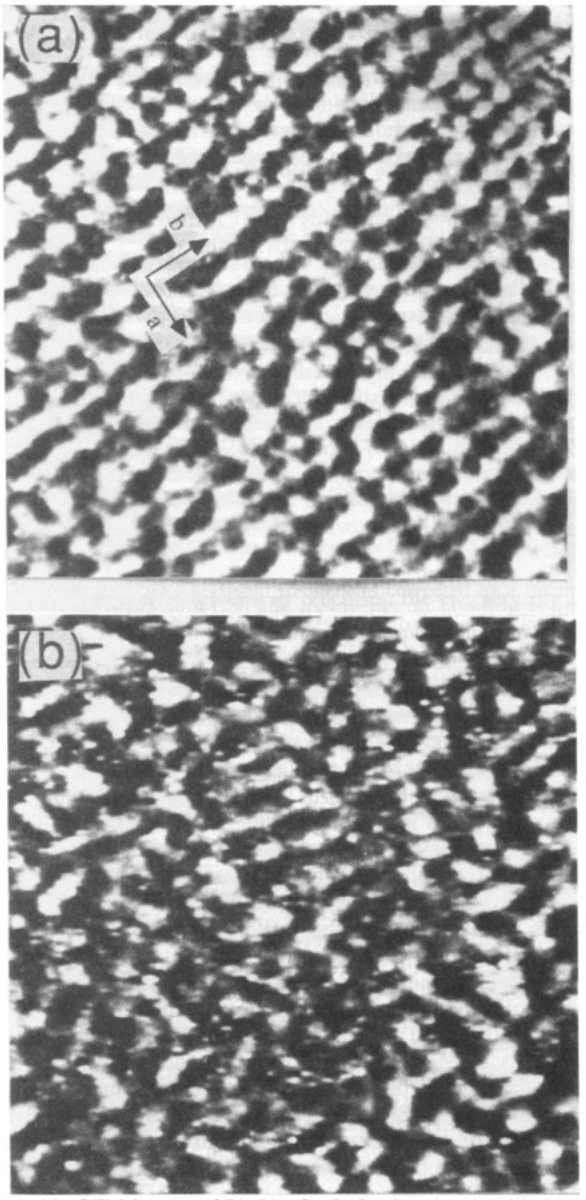

Figure 11. STM images of $Pb_xBi_{2-x}Sr_2CaCu_2O_8$ crystals with (a) x = 0.3 and (b) x = 0.7. These 480 × 480 Å^2 images were recorded with bias voltages/tunneling currents of 340/0.7 and 400 mV/0.8 nA, respectively. The a–b cell axes are marked in (a).

also show that the one-dimensional superstructure is less regular than in $Bi_2Sr_2CaCu_2O_8$ as evidenced by the random displacements along the a axis.[36] The distortions of the superlattice are likely due to the random substitution of Pb for Bi in the Bi(Pb)O planes and the resulting differences in PbO versus BiO bonding. Significantly, distortions in the superstructure imaged directly by STM explain the decrease in correlation length reported in diffraction studies of these materials; that is, random fluctuations along a (due to Pb substitution) reduce the scattering coherence. Further support of our suggestion that Pb substitution distorts the superlattice is found in images of the x(Pb) = 0.7 samples (Figure 11). These data exhibit a structural modulation on a 20–30-Å scale, although this modulation is highly disordered. Since similar disorder has been observed in images of x(Pb) = 0.7 crystals grown under a variety of conditions, it is apparent that this disorder is representative of the intrinsic structure of these heavily doped materials.

In addition, it is interesting to compare our microscopic STM data and measurements of T_c and the critical current density (J_c). Magnetization and resistivity measurements demonstrate that T_c is essentially unchanged by Pb substitution for x(Pb) ≤ 0.7. Since our STM data indicate that Pb substitution causes significant structural disorder in the Bi(Pb)O layer, we conclude that such

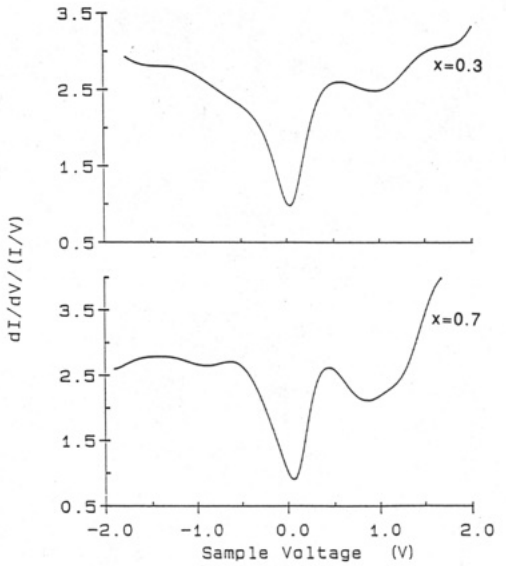

Figure 12. Plots of the normalized conductivity vs voltage corresponding to x = 0.3 and 0.7 $Pb_xBi_{2-x}Sr_2CaCu_2O_8$. The DOS at +1 V decrease as the concentration of Pb in the BiO layer increases.

disorder does not strongly perturb the electronic states near E_f (i.e., those states most important in determining T_c). To address the nature of the electronic states directly, we have made STS measurements on a series of Pb-substituted single crystals. Significantly, we find that the DOS near E_f are essentially unperturbed by Pb doping, although the electronic states at higher energy are affected by Pb incorporation into the lattice (Figure 12).[36,38] The normalized conductivity vs V data show that Pb causes a pronounced decrease in the empty DOS 1 eV above E_f. The fact that T_c remains unchanged, despite this decrease, shows that these electronic states are sufficiently removed energetically from E_f (and perhaps spatially from the CuO layer) that they do not interact with the electronic states near E_f critical in determining superconductivity. Substitution of other metals that perturb the electronic states of the BiO layer closer to E_f should serve as an important test of this idea.

Of perhaps greater significance is the insight that the local STM structural data provide in understanding variations in J_c with Pb substitution. We have recently shown that substitution of Pb causes reproducible and significant enhancements in J_c in $Pb_xBi_{2-x}Sr_2CaCu_2O_8$ materials.[48] While it is well known that crystal "defects" can enhance pinning of the flux line lattice, and hence increase J_c, the nature of the defects that cause pinning is not well understood in the HTSCs. In the Pb-substituted materials STM images have shown that Pb induces disorder in the one-dimensional superstructure, and correspondingly, J_c increases systematically with this disorder. We have suggested that the key defect in this system which enhances flux pinning is this superstructure disorder. Low-temperature STM measurements made in a magnetic field should address this key issue by directly defining the location of the flux lines in the crystal lattice.[49]

VI. Oxygen Doping in $Bi_2Sr_2CaCu_2O_x$

The second general example of substitution in the HTSCs that we will discuss is oxygen doping. It is widely recognized that oxygen doping plays a key role in determining the properties of oxide superconductors.[50-52] For example, the results from a number of studies have shown that variations in oxygen concentration change the average carrier concentration and thereby T_c.

(48) Wang, Y. L.; Wu, X. L.; Chen, C. C.; Lieber, C. M. *Proc. Natl. Acad. Sci.* **1990**, *87*, 7058.
(49) Zhang, Z.; Dai, H.; Lieber, C. M. Work in progress.
(50) Cava, R. J. *Science* **1990**, *247*, 656.
(51) Daeumling, M.; Seuntjens, J. M.; Larbalestier, D. C. *Nature* **1990**, *346*, 332.
(52) Jorgensen, J. D.; Pei, S.; Lightfoot, P.; Shi, H.; Paulikas, A. P.; Veal, B. W. *Physica C* **1990**, *167*, 571.

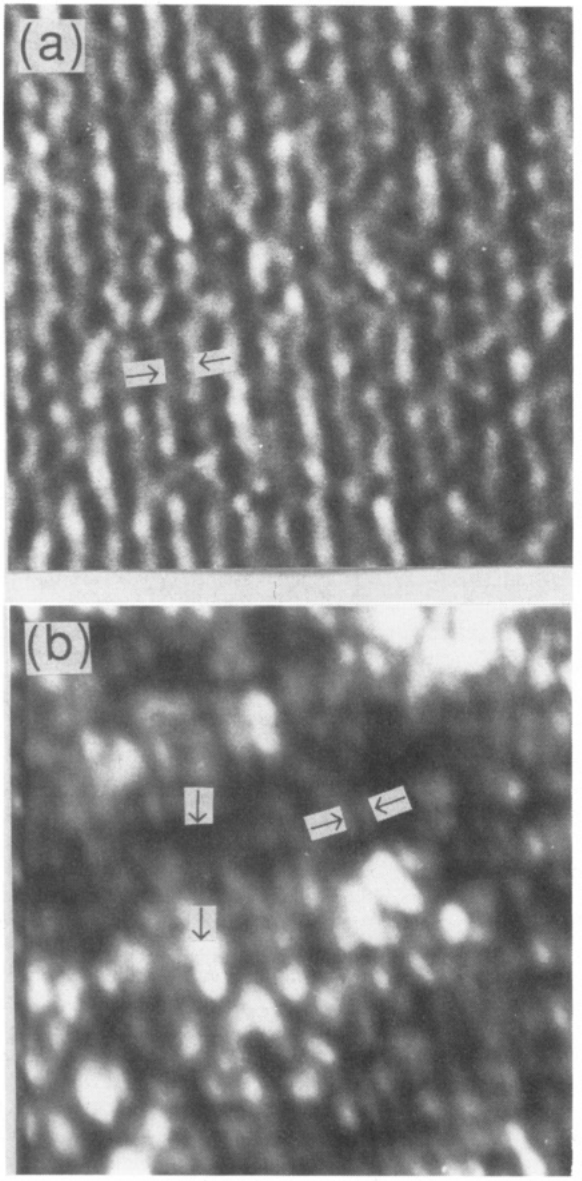

Figure 13. A 450 × 450 Å^2 image of a nonsuperconducting $Bi_2Sr_2CaCu_2O_8$ recorded with (a) $V = 900$ mV and (b) $V = 150$ mV. Two arrows mark adjacent maxima of the superstructure which are separated by about 25 Å in (a) and (b). Irregular electronic features at low bias are highlighted by additional arrows in (b).

More striking are, however, observations suggesting that small oxygen rearrangements can lead to superconductivity and enhanced fractions of superconducting material even when the average oxygen stoichiometry remains constant.[52] To understand these important effects, it is essential to characterize variations in the atomic structure and local electronic structure due to oxygen doping. Determination of the structure including oxygen positions is inherently difficult by diffraction techniques, although recent neutron scattering studies have provided insight into oxygen positional variations in $YBa_2Cu_3O_{7-\delta}$.[52] To date, changes in the microstructure associated with oxygen doping in $Bi_2Sr_2CaCu_2O_8$ have not been addressed, although it has been assumed that oxygen doping occurs in the BiO layer. Spatial variations in the electronic properties due to oxygen doping, which are especially important in these short coherence length materials, have not been characterized in either $Bi_2Sr_2CaCu_2O_8$ or $YBa_2Cu_3O_{7-\delta}$.

To begin to address this important problem, we have used STM to characterize the local structural and electronic changes that occur in vacuum-annealed $Bi_2Sr_2CaCu_2O_x$ crystals.[53] Vacuum annealing yields systematic decreases in T_c due to removal of oxygen from the crystals. STM images recorded on nonsuperconducting samples from which ≈3% oxygen was removed are shown in Figure 13. These images were recorded at 900 and 150 mV by switching the bias voltage on alternate scan lines; the two images are thus recorded in the identical spatial location. The image recorded at high V exhibits the one-dimensional superstructure characteristic of $Bi_2Sr_2CaCu_2O_8$. Notably, the superstructure period is unchanged in oxygen-deficient nonsuperconducting samples compared to $Bi_2Sr_2CaCu_2O_8$. These results indicate either that oxygen removed from the samples does not come from the BiO layer or that oxygen loss from this layer has little effect on the superstructure. To address the structural location of oxygen loss more directly, we have compared atomic-resolution images of the BiO layer of nonsuperconducting and superconducting crystals (Figure 14).[53] Images of the BiO layer of the oxygen-deficient crystals do not exhibit vacancies, and thus it is possible that oxygen is lost from the SrO or CuO layers. Studies to resolve this important issue are in progress.

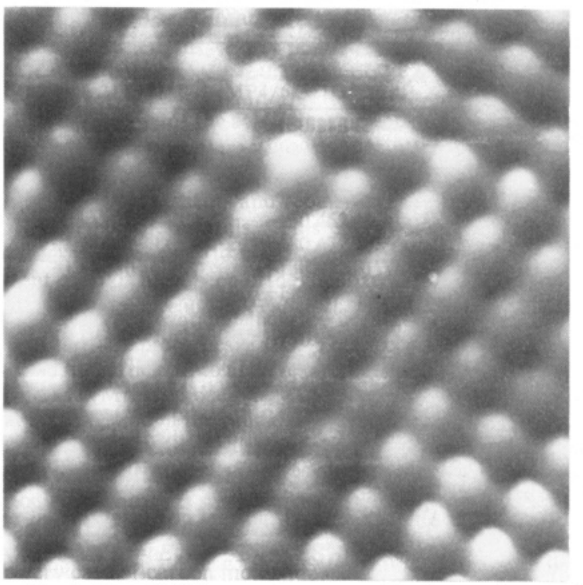

Figure 14. A 40 × 40 Å^2 image a nonsuperconducting sample recorded with a bias voltage of 275 mV and a tunneling current of 1.2 nA.

Images recorded at small V provide important additional information about the electronic effects of oxygen loss. Specifically, these data exhibit nonperiodic features in addition to a contribution from the one-dimensional superlattice. Analysis of images acquired over a range of V shows that the superstructure has the same spatial location irrespective of V and thus represents a true structural feature. The fact that the irregular features are only observed for small V indicates that these features are due to variations in the electronic states near E_f. Since the low bias voltage electronic states are not observed in images of superconducting samples, we conclude that they reflect spatial variations in the electronic properties due to oxygen loss. These electronic variations occur on the same scale as the coherence length (≈20 Å) and thus may affect pairing in intermediate-T_c crystals. In addition, we are currently investigating $Bi_2Sr_2CaCu_2O_x$ crystals annealed in high-pressure oxygen. STM studies of these materials show that the structure and electronic states of the BiO layer are also modified significantly by incorporation of additional oxygen into the lattice as discussed in detail elsewhere.[54]

VII. Low-Temperature Experiments

The energy gap, Δ, is one of the most fundamental properties characterizing a superconductor. For conventional superconductors, tunneling spectroscopy using planar junctions has been one of the most effective experimental techniques used to characterize the energy gap and DOS near E_f.[55,56] In terms of the

(53) Zhang, Z.; Wang, Y. L.; Wu, X. L.; Huang, J. L.; Lieber, C. M. *Proc. 2nd World Congress Supercond.*, Houston, in press. Wu, X. L.; Wang, Y. L.; Zhang, Z.; Lieber, C. M. *Phys. Rev. B* **1991**, *43*, 8729.

(54) Zhang, Z.; Lieber, C. M. Submitted for publication.

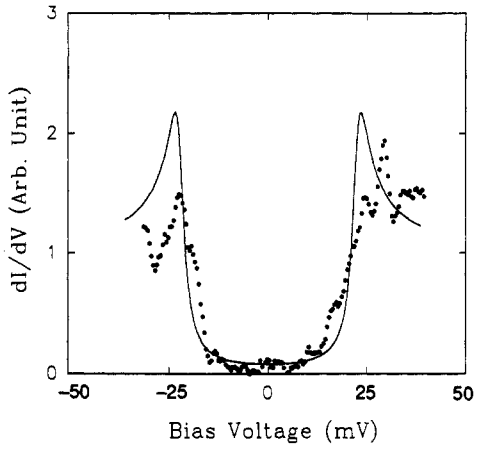

Figure 15. dI/dV vs V curve (solid dots) recorded on a $Bi_2Sr_2CaCu_2O_8$ crystal at 4.2 K. The solid line corresponds to the best fit of the data using eq 12 with $\Delta = 22.5$ and $\Gamma = 3.5$ meV.

standard weak coupling theory of Bardeen–Cooper–Schrieffer (BCS)[57] the tunneling DOS, dI/dV, in the superconducting state is given by

$$dI/dV = \mathrm{Re}\,\{(eV - i\Gamma)/[(eV - i\Gamma)^2 - \Delta^2]^{1/2}\} \quad (12)$$

where Γ is a broadening parameter that accounts for scattering processes which introduce states within the energy gap. In addition, within the context of BCS theory it is possible to define a reduced energy gap (i.e., Δ scaled by T_c) that has a universal value for weakly coupled superconductors: $2\Delta/k_BT_c = 3.53$.

In principle, the high spatial resolution of STM should provide a unique opportunity to characterize Δ, although studies to date have reported a wide range of values. A large part of these variations can be attributed to poor surface preparation as well as sample inhomogeneities. Hence, successful STM vacuum tunneling measurements of Δ require at least a clean and noninsulating surface. Cleaved surfaces of $Bi_2Sr_2CaCu_2O_8$ meet the first criteria; however, room temperature STM spectroscopic studies have shown that these surfaces are semiconducting.[37-39] This latter characteristic has made it difficult to obtain stable vacuum tunneling and measure Δ for $T < T_c$.

Recently, we have made considerable progress in obtaining reliable measurements of Δ on modified $Bi_2Sr_2CaCu_2O_8$ crystals and on $Tl_2Ba_2Ca_2Cu_3O_{10}$ crystals that have metallic surfaces. A typical plot of the DOS versus V obtained in the superconducting state for a $Bi_2Sr_2CaCu_2O_8$ sample at 4.2 K is shown in Figure 15. Notably, when the sample is cooled below T_c a well-defined gap develops in the DOS. To determine the value of Δ, we have fit this curve to a broadened BCS expression (12). The fit yields a value of Δ of 22.5 meV, and the value of the reduced energy gap calculated for this $T_c = 85$ K sample is 6.4. Similar values for the reduced energy gap have been obtained on $Tl_2Ba_2Ca_2Cu_3O_{10}$ crystals ($T_c \approx 120$ K). While these experiments are still at an early stage, the results are quite promising since they suggest that we will be able to determine the magnitude, temperature dependence, and spatial variation of Δ in HTSC materials when key experimental constraints are met.

VIII. Conclusions and Future Outlook

In this article we have shown how STM can provide unique insight into the structural and electronic properties of HTSC materials. In particular, these studies have (1) elucidated local structural disorder in BiO and TlO layers and the low-energy electronic states associated with this structure disorder, (2) characterized the structural and electronic effects of Pb and oxygen doping in $Bi_2Sr_2CaCu_2O_8$ materials, and (3) determined the magnitude of the superconducting energy gap in the $Bi_2Sr_2CaCu_2O_8$ and $Tl_2Ba_2Ca_2Cu_3O_{10}$ single crystals. We believe that these results represent the beginnings of a detailed microscopic picture for these highly complex materials and suggest that continued studies will lead to a much clearer understanding of superconductivity. Several particularly important areas of study for the future will be the following:

(1) To characterize the local structural and electronic effects of metal substitution and correlate these results with the observables T_c and J_c. Such studies could provide an "atomic level database" that is needed to rationally design improved HTSCs.

(2) To determine systematically the magnitude, temperature dependence, and spatial dependence of Δ. To understand the mechanism of superconductivity in these materials requires that Δ be reliably defined. We believe that it is especially necessary to elucidate whether local structural disorder affects Δ since these results will have important implications in understanding the nature of pairing.

(3) To characterize the nature of magnetic flux line lattice and the atomic details of flux pinning in the HTSCs. Such results are essential at this time to understand and to devise new methods for increasing J_c in these materials. In a more general sense STM can also provide essential microscopic data useful for understanding other problems in condensed matter science, and thus we believe that new applications of STM in this area hold great promise for the future.

Acknowledgment. We acknowledge contributions to the studies discussed in this article by J. L. Huang, Y. L. Wang, C. C. Chen, H. Dai, and X. L. Wu. C.M.L. thanks the David and Lucile Packard, National Science, Camille and Henry Dreyfus, and A. P. Sloan Foundations for generous support of this work.

(55) Wolf, E. L. *Principles of Tunneling Spectroscopy*; Oxford University Press: New York, 1989.
(56) Kirtley, J. R. *J. Mod. Phys. B* **1990**, *4*, 201.
(57) Bardeen, J.; Cooper, L. N.; Schrieffer, J. R. *Phys. Rev.* **1957**, *108*, 1175.